

Chapter 27

High-Order Discontinuous Galerkin Methods by GPU Metaprogramming

Andreas Klöckner, Timothy Warburton and Jan S. Hesthaven

Abstract Discontinuous Galerkin (DG) methods for the numerical solution of partial differential equations have enjoyed considerable success because they are both flexible and robust: They allow arbitrary unstructured geometries and easy control of accuracy without compromising simulation stability. In a recent publication, we have shown that DG methods also adapt readily to execution on modern, massively parallel graphics processors (GPUs). A number of qualities of the method contribute to this suitability, reaching from locality of reference, through regularity of access patterns, to high arithmetic intensity. In this article, we illuminate a few of the more practical aspects of bringing DG onto a GPU, including the use of a Python-based metaprogramming infrastructure that was created specifically to support DG, but has found many uses across all disciplines of computational science.

27.1 Introduction

Discontinuous Galerkin methods [5, 10, 17, 24] are, at first glance, a rather curious combination of ideas from Finite-Volume and Spectral Element methods. Up close, they are very much high-order methods by design. But instead of perpetuating the order increase like conventional global methods, at a certain level of detail, they switch over to a decomposition into computational elements and couple these el-

Andreas Klöckner
Courant Institute of Mathematical Sciences, New York University, New York, NY 10012, e-mail: kloeckner@cims.nyu.edu

Tim Warburton
Department of Computational and Applied Mathematics, Rice University, Houston, TX 77005 e-mail: timwar@caam.rice.edu

Jan S. Hesthaven
Division of Applied Mathematics, Brown University, Providence, RI 02912 e-mail: jan.hesthaven@brown.edu

ements using Finite-Volume-like surface Riemann solvers. This hybrid, dual-layer design allows DG to combine advantages from both of its ancestors. But it adds a third advantage: By adding a movable boundary between its two halves, it gives implementers an added degree of flexibility when bringing it onto computing hardware.

Using graphics processors for computational tasks is by no means a new idea. In fact, even in the days of marginally programmable fixed-function hardware, some (especially particle-based) methods obtained large performance gains from running on early GPUs. (e.g. [18]) In the domain of solvers for partial differential equations, Finite-Difference Time-Domain (FDTD) methods are a natural fit to graphics processors and obtained high performance with relative ease (e.g., [15]). Finite Element solvers were also brought onto GPUs relatively early on (e.g., [9]), but often failed to reach the same impressive speed gains observed for the simpler FD methods. In the last few years, high-level abstractions such as Brook and Brook for GPUs [3] have enabled more and more complex computations on streaming hardware. Building on this work, Barth et al. [1] already predicted promising performance for two-dimensional DG on a simulation of the Stanford Merrimac streaming architecture [6]. Nowadays, compute abstractions are becoming less encumbered by their graphics heritage [19, 22]. This has helped bring algorithms of ever higher complexity onto the GPU. Taking advantage of these advances, our paper [12] presented, to the best of our knowledge, the first implementation of a discontinuous Galerkin method on a single real-world consumer graphics processor. Now, a few years after the publication of the original paper, interest in GPUs and their use for solving partial differential equations continues unabated. A few implementers have followed in our footsteps and brought their versions of DG onto GPUs.

Let us briefly place this text within the sequence of articles on GPU-DG we have authored. The first one [12] is rather technical and introduces all the tricks and details needed to make the method go fast. The second one [13] serves as an introduction to be read by a larger, somewhat non-technical audience. This latest one addresses some of the software challenges involved in achieving fast execution of GPU-based discontinuous Galerkin methods.

The article is structured as follows: In Section 27.2, we review the details of the discontinuous Galerkin method and its implementation in general, followed by a discussion of considerations required by its implementation on GPUs specifically in Section 27.3. Responding to the challenges of this section, we introduce the motivation and implementation details of our Python-based infrastructure for run-time code generation (RTCG) in Section 27.4. We then discuss the specifics of RTCG in the context of DG in Section and confirm the success of the method through experimental results in Section 27.5. In closing and summing up what was achieved, we outline avenues for future work in Section 27.6.

27.2 The Discontinuous Galerkin Method

By their design and origins, DG methods are particularly suited to approximating the solution of a hyperbolic system of conservation laws

$$u_t + \nabla \cdot F(u) = 0. \quad (27.1)$$

Initial boundary value problems for PDEs that can be cast in the form (27.1) as well as slight generalizations thereof, include Maxwell's equations, Euler's equations of gas dynamics, the Navier-Stokes equations, equations arising from Lattice-Boltzmann models, the equations of magnetohydrodynamics, or the shallow-water equations. In summary, a wide variety of physical phenomena in the time domain can be modeled using this type of equation.

(27.1) is to be solved on a domain $\Omega = \biguplus_{k=1}^K D_k \subset \mathbb{R}^d$ consisting of disjoint, face-conforming tetrahedra D_k with boundary conditions

$$u|_{\Gamma_i}(x,t) = g_i(u(x,t), x, t), \quad i = 1, \dots, b,$$

at inflow boundaries $\biguplus \Gamma_i \subseteq \partial\Omega$. As stated, we will assume the flux function F to be linear. We find a weak form of (27.1) on each element D_k :

$$\begin{aligned} 0 &= \int_{D_k} u_t \varphi + [\nabla \cdot F(u)] \varphi \, dx \\ &= \int_{D_k} u_t \varphi - F(u) \cdot \nabla \varphi \, dx + \int_{\partial D_k} (\hat{n} \cdot F)^* \varphi \, dS_x, \end{aligned}$$

where φ is a test function, and $(\hat{n} \cdot F)^*$ is a suitably chosen numerical flux in the unit normal direction \hat{n} . Following [10], we find a 'strong'-DG form of this system as

$$0 = \int_{D_k} u_t \varphi + [\nabla \cdot F(u)] \varphi \, dx - \int_{\partial D_k} [\hat{n} \cdot F - (\hat{n} \cdot F)^*] \varphi \, dS_x. \quad (27.2)$$

We seek to find a numerical vector solution $u^k := u_N|_{D_k}$ from the space $P_N^r(D_k)$ of local polynomials of maximum total degree N on each element. We choose the scalar test function $\varphi \in P_N(D_k)$ from the same space and represent both by expansion in a basis of $N_p := \dim P_N(D_k)$ Lagrange polynomials l_i with respect to a set of interpolation nodes [26]. We define the mass, stiffness, differentiation, and face mass matrices

$$M_{ij}^k := \int_{D_k} l_i l_j \, dx, \quad (27.3a)$$

$$S_{ij}^{k,\partial v} := \int_{D_k} l_i \partial_{x_v} l_j \, dx, \quad (27.3b)$$

$$D^{k,\partial v} := (M^k)^{-1} S^{k,\partial v}, \quad (27.3c)$$

$$M_{ij}^{k,A} := \int_{A \subset \partial D_k} l_i l_j \, dS_x. \quad (27.3d)$$

Using these matrices, we rewrite (27.2) as

$$0 = M^k \partial_t u^k + \sum_{\mathbf{v}} S^{k, \partial_{\mathbf{v}}} [F(u^k)] - \sum_{F \subset \partial D_k} M^{k,A} [\hat{n} \cdot F - (\hat{n} \cdot F)^*],$$

$$\partial_t u^k = - \sum_{\mathbf{v}} D^{k, \partial_{\mathbf{v}}} [F(u^k)] + L^k [\hat{n} \cdot F - (\hat{n} \cdot F)^*]_{A \subset \partial D_k}. \quad (27.4)$$

The matrix L^k used in (27.4) deserves a little more explanation. It acts on vectors of the shape $[u^k|_{A_1}, \dots, u^k|_{A_4}]^T$, where $u^k|_{A_i}$ is the vector of facial degrees of freedom on face i . For these vectors, L^k combines the effect of applying each face's mass matrix, embedding the resulting facial values back into a volume vector, and applying the inverse volume mass matrix. Since it “lifts” facial contributions to volume contributions, it is called the *lifting matrix*. Its construction is shown in Figure 27.1.

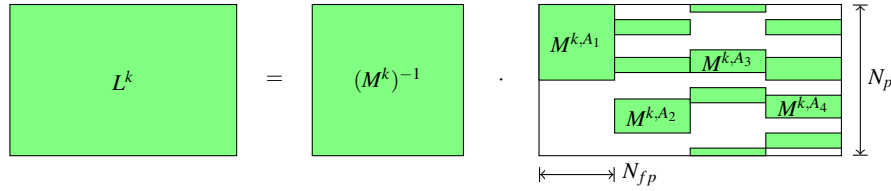


Fig. 27.1 Construction of the Lifting Matrix L^k .

It deserves explicit mention at this point that the left multiplication by the inverse of the mass matrix that yields the explicit semidiscrete scheme (27.4) is an element-wise operation and therefore feasible without global communication. This strongly distinguishes DG from other finite element methods. It enables the use of explicit (e.g., Runge-Kutta) time stepping and greatly simplifies parallel implementation efforts such as this one.

27.2.1 Implementing DG

DG decomposes very naturally into four stages, as visualized in Figure 27.2. This clean decomposition of tasks stems from the fact that the discrete DG operator (27.4) has two additive terms, one involving an element volume integral, the other an element surface integral. The surface integral term then decomposes further into a ‘gather’ stage that computes the term

$$[\hat{n} \cdot F(u_N^-) - (\hat{n} \cdot F)^*(u_N^-, u_N^+)]_{A \subset \partial D_k}, \quad (27.5)$$

and a subsequent lifting stage. The notation u_N^- indicates the value of u_N on the face A of element D_k , u_N^+ the value of u_N on the face opposite to A .

As is apparent from the use of a Lagrange basis, we employ a *nodal* version of DG, in which the stored degrees of freedom (“DOFs”) represent the values of u_N at a set of interpolation nodes. This representation allows us to find the facial values used in (27.5) by picking the facial nodes from the volume field. (This contrasts with a *modal* implementation in which DOFs represent expansion coefficients in a non-Lagrange basis. Finding the facial information to compute (27.5) requires a different approach in these schemes.)

Observe that most of DG’s stages are *element-local* in the sense that they do not use information from neighboring elements. Moreover, these local operations are often efficiently represented by a dense matrix-vector multiplication on each element.

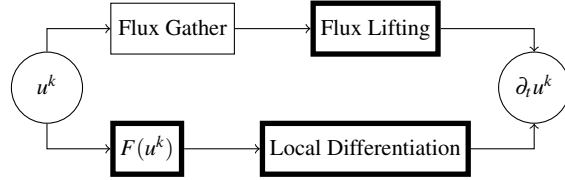


Fig. 27.2 Decomposition of a DG operator into subtasks. Element-local operations are highlighted with a bold outline.

It is worth noting that since simplicial elements only require affine transformations Ψ_k from reference to global element, the global matrices can easily be expressed in terms of reference matrices that are the same for each element, combined with scaling or linear combination, for example

$$M_{ij}^k = \underbrace{\left| \det \frac{d\Psi_k}{dr} \right|}_{J_k :=} \underbrace{\int_{\mathcal{I}} l_i l_j dx}_{M_{ij} :=}, \quad (27.6a)$$

$$S_{ij}^{k,\partial v} = J_k \sum_{\mu} \frac{\partial \Psi_v}{\partial r_{\mu}} \underbrace{\int_{\mathcal{I}} l_i \partial_{r_{\mu}} l_j dx}_{S_{ij}^{\partial \mu} :=}, \quad (27.6b)$$

where $\mathcal{I} = \Psi_k^{-1}(\mathcal{D}_k)$ is a reference element. We define the remaining reference matrices D , M^A , and L in an analogous fashion.

27.3 GPU-DG: Motivation and Challenges

As we begin our study of bringing DG methods onto GPU-like architectures, we should first establish what we intend to achieve in doing so. Our main motivation is a gain in performance available from a desk-side workstations. We believe that

the amount of computing power easily available to an engineer often determines the amount of computing power used in a given engineering challenge. Remote resources such as big clusters provide large amounts of power quite readily, but their use also implies a complexity burden in management, cost, and access. Nonetheless, good performance on clusters and large machines is clearly a secondary goal. Next, we would like to be able to apply the technology under discussion to a wide range of partial differential equations. While DG methods are designed for and best suited to hyperbolic PDEs, there is no conceptual restriction to this type of PDE—and our GPU-DG technology is not restricted in this way, either. A tertiary goal of ours is to make the technology not just worthwhile on a desk-side workstation, but also simple enough to apply that an engineer can easily manage his or her own computations. While this is partially a software design issue beyond the scope of this article, some prerequisites at the GPU computation level must be met to accommodate the desired ease of use. In particular, no knowledge of GPU computing is necessary to manage a computation.

The discontinuous Galerkin method further allows considerable user choice at the level of the reference discretization. It is not practical to support *all* such choices, and thus we introduce the following (fairly non-restrictive) stipulations:

- We will specialize to straight-sided simplices, as we perceive the required volume mesh generation machinery to be the most mature for this type of element. The restriction to straight-sidedness is comparatively easy to lift [27].
- We will optimize for (but not specialize to) the three-dimensional case, i.e. tetrahedral elements, as it bears both the most relevance to application problems and the greatest computational complexity.
- We will further optimize for “medium” order ($N = 3 \dots 5$) polynomial spaces, as those maintain the DG time step restriction ($\Delta t \sim \Delta x/N^2$, see [10]) at a reasonable level.

Next, we consider what possible obstacles our effort to bring DG to the GPU may face. Perhaps the first challenge that comes to mind is that of data movement. As in any matrix-product-type workload, there is much data reuse in DG, but matrices grow rapidly as N increases. In terms of data reuse, that is good—however it does compete with the limited size of on-chip memories that are needed to realize the possible reuse. Further, while on-chip memories are growing at a moderate pace and management of these memories becomes more automatic, it should be noted that even CPU-based matrix-matrix multiplies benefit from explicit management of their L1 caches [2, 28] in matrix-based workloads. Strongly interwoven with the challenge of having to manage on-chip memories is that of accommodating hardware granularities, such as memory sizes, memory bus widths, SIMD widths, work-group sizes, and so on. In addition, discontinuous Galerkin methods have their own preferred granularities, such as the number of degrees of freedom in each element, the number of dimensions, or the number of degrees of freedom on an element’s face. Unfortunately, while machine-related granularities have a tendency to be powers of two, the exact opposite is true of those related to the numerical method. Another challenge posed by GPU computing is the necessity to map the computation

onto a two-level, grid-based parallel execution structure, with the first level corresponding to parallelization across cores, and the second to parallelization across SIMD lanes within a core. While a coarse-grain structure may often be immediate, various finer details of this choice require careful tuning.

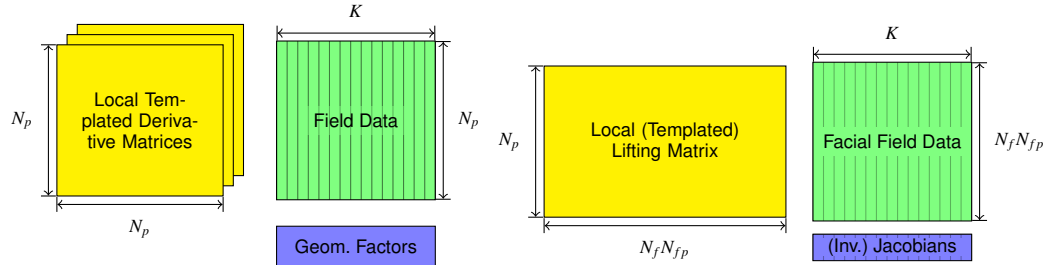


Fig. 27.3 Workload size characterization for element-local linear operators. Left: Element-local differentiation. Right: Lifting from flux values along element faces into volume data. In each case, matrix sizes are given in terms of the quantities of Section 27.2.

We will now discuss how these challenges are met by our approach, through a few representative examples, beginning with the question of data movement for element-local linear operators such as lifting and elementwise differentiation. Figure 27.3 illustrates the type and size of data that these procedures operate on. The figure also makes it obvious that while the method primarily relies on matrix-vector products, it is profitable to view the field vectors in aggregate as a matrix, thereby giving rise to a matrix-matrix computation, albeit with very off-balance matrix dimensions. An obvious first approach would be to use vendor-supplied BLAS matrix libraries for such a task, however it turns out that these are often tuned for large, square matrices and rarely deal well with the matrix sizes occurring in DG. One is therefore left to build a home-grown algorithm. Given that, depending on the local polynomial order N , only a limited amount of this data can fit onto the chip, the implementer is faced with a decision of which data to store locally and which data to stream onto the chip. In particular, one might consider the following alternatives:

- Store the matrices, stream the vector data. This seems like an obvious choice—however the matrices are often too large, and vector data is much more easily partitioned.
- Store part of a matrix. This complicates the access logic, but can often profitably be done—especially by using row-wise partitions.
- Store only field data. If streaming of the matrix is achieved through a cached data path, this can also be an attractive option.
- Store parts of the matrix and the field vector. While this could, in theory, provide the best balance of data reuse, we were unable to turn this approach into competitive code.

This is a choice that an implementer needs to make, however we have found no universally valid heuristic that might provide guidance on which alternative to choose,

especially given that the optimality of each option strongly depends on the hardware being used.

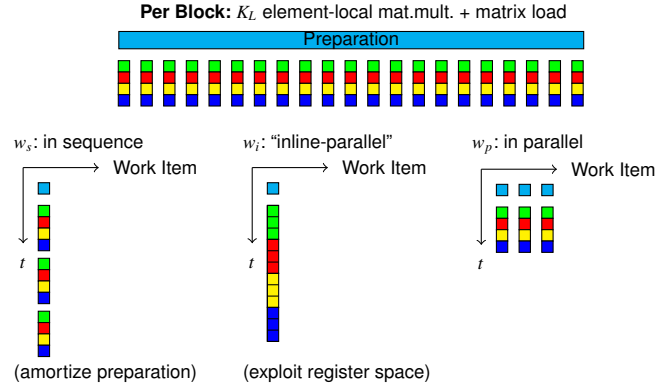


Fig. 27.4 Choices for the amount of work done by a workgroup in an element-local (differentiation, lift) operation.

For the same workload of elementwise local differentiation and lifting, there is also the question of which work decomposition to use, where the work decomposition is given (in vendor-neutral OpenCL terminology) by the number of workgroups and their sizes. Each of these quantities can further be decomposed into a three-component vector. Order in this three-component vector matters, as it determines which work items execute memory accesses at the same time, and which branches may require serialization.

Abstractly, the workload under consideration consists of an (optional) preparatory step that preloads matrix data into on-chip memory, followed by dot products for each matrix row and all the columns (field vectors). The most immediate choice would be to have each workgroup deal with one such matrix-vector product, leading to a one-to-one mapping between workgroups and DG elements. While this is certainly straightforward, it has a number of drawbacks. For the polynomial orders N targeted in this work, these workgroup sizes are unable to fill the (32- or 64-)wide SIMD architectures exhibited by today's GPUs—at least not efficiently, and not without leaving unused 'gaps' in the SIMD vector. Further, one also typically adds padding to conform to a device's memory alignment, and this choice leads to a maximum number of gaps in the data, thereby wasting a considerable amount of (typically precious) GPU memory. In addition to that, if one workgroup only performs one matrix-vector product, any preparation steps would be poorly amortized.

Irrespective of more advanced blocking options (as described in [12]), there are three basic, orthogonal (i.e. arbitrarily combinable) possibilities of remedying this situation, outlined in Figure 27.4. Two of these choices are entirely obvious, the third slightly less so. The obvious choices include letting a workgroup do more things *in sequence* and *in parallel*. The former of these leads to better amortization

of preparation steps, while the latter does that, and in addition increases utilization of parallel processing resources. The third choice, called *in-line parallel* in Figure 27.4, occupies a middle-ground between the two by accomplishing a number of dot products along with each other within a single work item. This exploits the fact that, in order for the matrix to be operated on, its components must be resident within the GPU’s register file—but once they are there, it is economical to use them not just once, but multiple times. All of these strategies are specific forms of *work item coarsening*. How many elements are worked on in each of these fashions is captured by the numbers w_s , w_i and w_p .

Obviously, regardless of the choices for these numbers, the same amount of work is being done—it is just the partitioning that differs. Nonetheless, in Section 27.5, we will observe fairly significant performance differences between such partitionings.

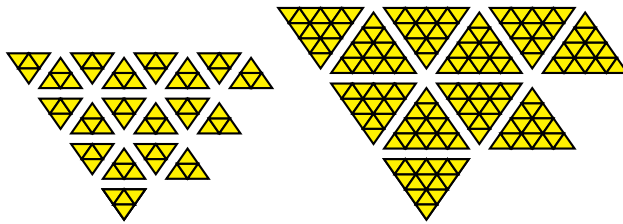


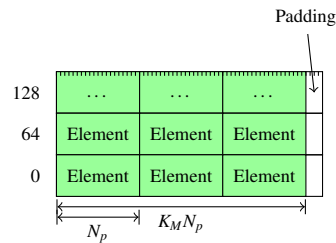
Fig. 27.5 Multiple granularities for inter-element flux computation. Obviously, larger blocks lead to more data reuse as fewer face pairs are split.

We have just seen that a question of granularities arises even in a simple situation like that of the element-local operations. There is an even more important concern of this nature in the only inter-element communication operation within DG, the computation of surface fluxes. Since the computation of each surface flux refers to data from two opposite element faces, there is definite savings potential if data for a number of such faces is brought onto the chip at the same time and reused. Obviously, this leads to a decrease in the amount of parallelism available, but for large enough problems (which are the main driver for the application of GPU technology), this becomes a non-issue. The amount of parallelism is however limited by two sets of data that need to be fit onto the chip, namely the metadata indicating which faces with what geometry data need to be processed, and the output buffer used to write vectors of face data that can then be processed in the lifting stage of the computation. Both of these could theoretically be accomplished in streaming mode without on-chip storage, however we have found that buffering them improves performance measurably. Once a granularity has been found that suitably balances these factors with data reuse, the computational mesh needs to be partitioned in a way that maximizes the number of interior faces in each partition. Fortunately, we have found that performance is somewhat insensitive to the absolute quality of this partition, and a simple greedy algorithm, as outlined in [12], suffices.

Overall, we have seen a few examples of computations requiring that the implementer select a granularity entirely unrelated to the computation itself. Each of these

granularities is bound to want to manifest itself somehow in the in-memory data storage format, likely through coalescing/alignment concerns. On the other hand, it is *not* likely that a single data storage format can satisfy *all* restrictions of *all* parts of the computation. A compromise therefore needs to be made. In calling the granularities of each of the computations “*blocks*” (related to the Nvidia term for work-groups), we arrived at the idea of an intermediate granularity consisting of an integer number of elements and just big enough to satisfy the device’s basic alignment preference, but not necessarily conforming to any particular computation. This would then be called a “*microblock*” (illustrated in Figure 27.6), and we would demand that all the actual computation granularities be integer multiples of a microblock. A similar technique was independently discovered in [7]. Seemingly, this just introduces yet another semi-arbitrary number to be chosen before the computation can begin, but nonetheless its introduction does some good by relieving the tension over the data storage format between different parts of the computation.

Fig. 27.6 Element storage in “microblock” format as described in the text. An small, integer number of elements is followed by enough padding to satisfy device alignment requirements. Other computation granularities are specified as integer numbers of microblocks.



As we conclude our overview of a few of the challenges of bringing discontinuous Galerkin methods onto the GPU, we observe that there is a common theme uniting many of them—the answers are strongly hardware-dependent. This has a number of important consequences:

- The questions themselves are difficult to answer. Modern processor hardware tends to be very complicated, with many clock domains, bandwidth figures, possibilities for resource contention, and so on.
- Published information on hardware provides insufficient heuristics to make well-founded decisions on any of these.
- Even if a good answer to these questions existed, then it would not necessarily have any lasting value. Software tends to have a much longer shelf life than hardware, as new hardware revisions with programmer-visible changes to microarchitecture (in both the GPU and CPU markets) appear at a rate of about one every two years. Some things (such as the OpenCL programming model) are expected to be durable for at least some time, but the fine features determining tuning decisions such as those outlined above are subject to frequent change.

One obvious solution to this tuning dilemma stems from the realization that computer cycles are cheap—and that it is thus reasonable to let a computer help as much as possible in solving these challenges. If that means letting the machine try out a

large number of possible combinations of parameter settings, that is fine–computer time is less expensive than human time, and this trend will almost certainly continue. Furthermore, this shifts two aspects of GPU programming in the right direction. First, it shifts the programmer’s role from caring about tuning results to coming up with tuning ideas—and letting the computer determine to what extent those are effective. Second, it decreases the amount of detailed hardware knowledge necessary to come up with a high-performance program. Arguably, both of these represent steps in the right direction. In the next section, we will present ideas on the concrete implementation of *automated tuning*.

27.4 Run-Time Code Generation

The capability to do automated tuning, i.e. to do an automated benchmark of a large number of variants of a program turns out to be a special case of a much more general facility—that of *Run-Time Code Generation* (“RTCG”).

This phrase has two parts, ‘code generation’ and ‘run-time’. In itself, the *generation* of source code is merely a text processing task, and most modern languages, which most modern languages are more than capable of. What is being discussed here is thus not the actual generation of the code (which is just a piece of ASCII text), but rather the ability to compile and run this code in-process, at *run-time*.

GPU programming environments such Nvidia’s CUDA “runtime” interface make this difficult because they insist that all code be compiled ahead of time and into one final binary . In such a setting, all possible tuning variants must already be precompiled into the application binary. This restriction can of course be worked around using dynamic linking and/or shell scripting, but none of these lead to particularly elegant or robust solutions.

We aim to demonstrate in this article that *scripting languages* make a very hospitable environment for run-time code generation, especially when using interfaces such as OpenCL or the Nvidia CUDA “driver” interface which facilitate RTCG more easily. Scripting languages usually have no need for a user- or developer-visible compilation step, and thus everything they do is, by definition, done at run time.

Even beyond what was discussed so far, there are many good reasons to ask for the ability to do run-time code generation:

- *Automated Tuning*, as discussed. (This is also done, although in a variety of ways accommodating ahead-of-time compilation, by packages such as ATLAS [28], FFTW [8], or PHiPAC [2].)
- The ability to vary *data types* at run time. This might include the ability to run in double or single precision, with complex- or real-valued data, or even more complicated variants, such as interval arithmetic. Templates (in C++) partially address this need in the ahead-of-time-compiled world, however, they also incur the overhead of having to compile each possible variant into the executed binary, as there is no possibility for compilation at run time.

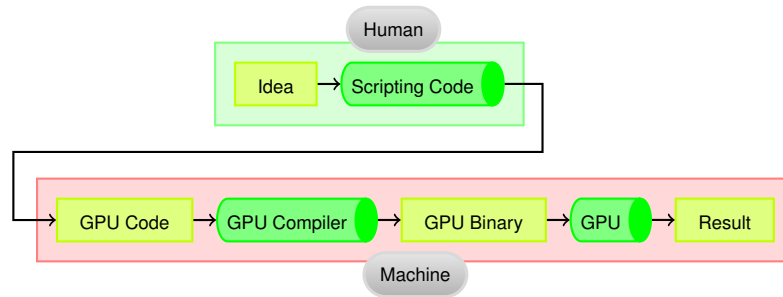


Fig. 27.7 Operating principle of GPU code generation.

- From the perspective of a library writer, another attractive possibility opened up by RTCG is the possibility to *specialize code for a user-given problem*. While many rather complicated systems involving C++ metaprogramming strive to achieve this goal, they cannot match the simplicity (and performance) of textually pasting a chunk of purpose-specific C code into an overall code framework. Also note that this benefit is really not specific to library writers at all. At some level, every programmer strives to write code that is general and covers a wide variety of use cases. RTCG opens up a very simple and high-performance avenue towards this goal.
- Lastly, it should be observed that *constants faster than variables*. This can be easily understood from the standpoint of *register pressure*—where space in the register file is just one of many resources that are scarce in a GPU, and less contention means that some trade-off does not need to be made, which usually results in higher performance. Another specific example of this is *loop unrolling*. Loops with unknown trip counts necessarily come with fixed overhead in the form of end-of-loop tests and branching instructions, in addition to loop-related state being kept in the register file. If the loop trip count is known at run-time, then this overhead is easily done away with.

All of these arguments in favor of RTCG rest on a simple fact: *More information is available to a code generator and compiler at run time than at any time before that*. And unsurprisingly, the more information is available to the code generator and the compiler, the better the code it is able to generate. Also observe that in this picture, the code generator and the compiler start to merge together conceptually, and the representation in which they exchange data (often a variant of C, for now) moves towards being an implementation detail. This is a good thing, as it makes it expedient for programmers to develop representations that best serve their application. Interfaces like CorePy [21] and LLVM [16] demonstrate that C is not the only possible intermediate representation.

As we discuss the advantages of RTCG, we should likely also mention the (in our opinion few and minor) disadvantages. First, RTCG obviously adds more moving parts (such as a compiler and a just-in-time execution environment) to a program, which introduces more possible sources of issues. Second, as generated code must

be compiled, there is often a noticeable delay before a piece of code is first executed. However, caching and parallel compilation are effective remedies for this.

Despite these perceived drawbacks, the creators of the OpenCL specification seem to agree with our point of view and have made RTCG a standard part of the OpenCL interface—which, in our opinion, is one of the most interesting contributions OpenCL makes to the high-performance computing arena. When OpenCL is compared to CUDA, one drawback that is often cited is OpenCL’s lack of support for C++ templates. This is a moot point, in our opinion, as RTCG is strictly more powerful than C++ templates.

Next, we would like to continue to argue that RTCG is most effective when practiced from a scripting language. Scripting languages are in many ways polar opposites to GPUs. GPUs are highly parallel, subject to hardware subtleties, and designed for maximum throughput. On the other hand, scripting languages (such as Python [25]) favor ease of use over computational speed, are largely hardware-agnostic, and do not generally emphasize parallelism. We have created two packages, PyOpenCL and PyCUDA [11], that join GPUs and scripting languages in one programming environment.

Before we move on, however, let us comment on a practicality: In today’s GPU programming environments (OpenCL, CUDA), all the host computer is required to do is submit work to the compute device at a certain rate, typically around 1000 Hz. As long as the scripting-based host program can maintain this rate, there is no loss in performance.

PyOpenCL and PyCUDA can be used in a large number of roles, for example as a prototyping and exploration tool, to help with optimization, as a bridge to the GPU for existing legacy codes (in Fortran, C, or other languages), or, perhaps most excitingly, to support an unconventional *hybrid way of writing high-performance codes*, in which a high-level controller generates and supervises the execution of low-level (but high-performance) computation tasks to be carried out on varied GPU- or GPU-based computational infrastructure.

Scripting languages already excel at text processing and are routinely used for this task at extreme scales, as exemplified by their use in the generation of HTML pages. This already makes them a good choice for the textual part of code generation. A number of further points contribute to making the programming environment created by joining GPUs and scripting greater than just the sum of its two parts. First, scripting languages lend themselves to very clean programming interfaces, with seamless (but invisible) error reporting and automatic resource management. In addition, scripting languages are very suited to creating abstractions, and Python especially follows a “batteries included” approach that puts many of these abstractions directly within a user’s reach. PyOpenCL and PyCUDA strive to make ideal use of these characteristics. They are fully documented, and also come with “batteries included”—for instance, users do not have to reinvent vectors, arrays, reductions or prefix sums. Both packages also cache compiler output, to support RTCG and retain the development “feel” of a scripting language.

The Python programming language [25] is well-suited for such packages for a number of reasons:

- The existence of a mature array abstraction (`numpy` [23]) facilitating (in-process) transport and manipulation of bulk numerical data.
- The large ecosystem of software that has sprung up around `numpy`.
- Its main-stream syntax and language-features, which make the language easy to learn while not impeding more advanced use.

Other languages may certainly be just as suitable.

In concluding this argument for GPUs, scripting and RTCG, let us remark that the packages introduced here are distributed under the liberal MIT license and are available at the URLs <http://mathematician.de/software/pyopencl> (or [/pycuda](http://mathematician.de/software/pycuda)). A mailing list, a wiki, and a number of contributed computational add-on packages are available. Both packages are routinely used on Windows, OS X, and Linux.

27.5 Results: RTCG for Discontinuous Galerkin

a)

$$\hat{n} \cdot (F - F^*)_E := \frac{1}{2} [\hat{n} \times (\llbracket H \rrbracket) - \alpha \hat{n} \times \llbracket E \rrbracket]$$

b)

```
flux = 1/2*cross(normal, h.int-h.ext
             -alpha*cross(normal, e.int-e.ext))
```

c)

```
a_flux += (
  ((( val_a.field5 - val_b.field5)*fpair->normal[2]
    - ( val_a.field4 - val_b.field4)*fpair->normal[0])
  + val_a.field0 - val_b.field0)*fpair->normal[0]
  - ((( val_a.field4 - val_b.field4) *fpair->normal[1]
    - ( val_a.field1 - val_b.field1)*fpair->normal[2])
  + val_a.field3 - val_b.field3) * fpair->normal[1]
)*value_type(0.5);
```

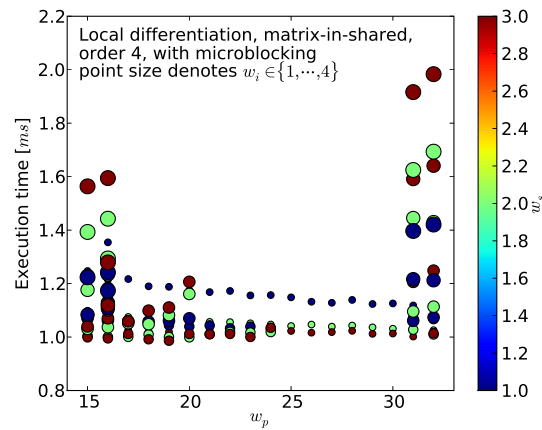
Fig. 27.8 Three representations of a (partial) numerical flux for the Maxwell equations. a) shows the mathematical specification as first given in [20]. b) shows the Python code used to instruct the solver. c) shows a fraction (about one sixth) of the C code ultimately generated by the solver to implement the flux in a).

Having introduced run-time code generation as a way of addressing the challenges encountered in Section 27.3, we will refocus on some of the specific benefits that RTCG brings in the context of a discontinuous Galerkin solver and discuss a few of the achieved results. For definiteness, we will be discussing results obtained using the solver “hedge”, which was built to explore and develop the ideas in this article.

The first example emphasizes the impact of RTCG on the ability to write maintainable software with reasonable user interfaces. In particular, we will demonstrate

the user interface that our DG solver code uses to specify numerical flux terms—the terms $(n \cdot F^*)$ in (27.2). Figure 27.8 shows three representations of a (partial) numerical flux for the Maxwell equation. First, Figure 27.8a) shows the mathematical notation as one might find in a scientific article. Next, Figure 27.8b) shows the Python code that a user might need to write to capture the numerical flux expression of a) in our solver. The final part c) of the figure shows a fraction of the generated code. What this seeks to demonstrate is that a high-performance, low-level, scalar C-language representation can easily be generated from a high-level, vectorial statement in a scripting language. It is obvious that the code in Figure 27.8b) is much easier to check for correctness than the resulting C code. Nonetheless, even textbooks such as [10] contain code like that of 27.8c) for demonstration purposes. By using RTCG, in many situations it becomes a rather easy proposition to enable the user to write maintainable, transparent code, and still obtain all the performance of a program that would have previously required a rather large amount of manual labor and checking.

Fig. 27.9 Sample tuning study for local differentiation on fourth-order elements with microblocking enabled, showing time spent for a constant amount of work depending on the values w_s , w_p and w_i introduced in Section 27.3.



Further, our solver obviously makes extensive use of automated tuning. Figure 27.9 shows results from a particular tuning run attempting to optimize the parameters w_s , w_p and w_i introduced in Section 27.3 for element-local differentiation. The vertical axis of the plot shows timing information, and each of the dots in the plot represents a particular timing run. The same amount of numerical work was done for each of the dots, yet surprisingly, the final performance varied by more than a factor of 2 depending on parameter choice. In addition, there is little observable regularity in the graph, which seems to limit the amount of success that any given heuristic might have in predicting this behavior. There is almost no other option besides automated tuning to find an at least somewhat optimal combination within this parameter space. Also note that any performance gain in this part of the operator has a rather large impact on the performance of the method as a whole—element-local differentiation is the asymptotically most work-intensive part of a DG operator.

In addition to this application of automated tuning in the determination of a parallel work decomposition, our solver also applies this technique in finding memory layouts and flux gather granularities. Further, by virtue of code generation, it naturally benefits from being able to “hard-code” certain variable values such as matrix sizes, polynomial degrees, or loop trip counts.

In the following, we will present a number of overall performance results for our solver on an Nvidia GTX 280, to confirm that a high-performance solver can be written using the techniques described. Unless otherwise specified, all performance numbers are based on the wall clock time from the beginning of one time step to the beginning of the next, including RK4 timestepping. Timings were averaged over a run of 100 (CPU) or several hundred (GPU) time steps to minimize the influence of timing transients. Timings were observed to be consistent across runs, even when using automated tuning.

Fig. 27.10 Floating point performance in GFlops/s achieved by our auto-tuning solver on a large 3D Maxwell problem in single precision on an Nvidia GTX 280. Performance is calculated by measuring wall time from one time step to the next and dividing the number of flops performed (including timestepping) by this value.

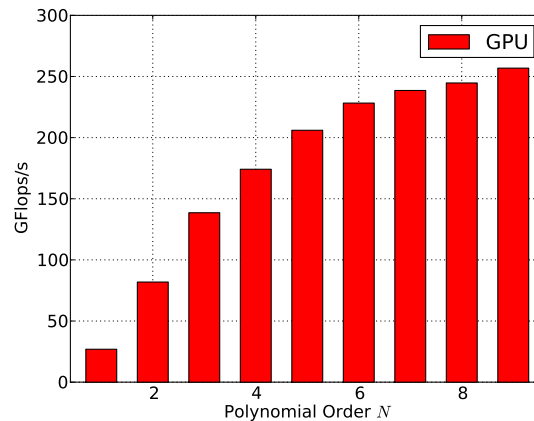


Figure 27.10 shows overall performance expressed in billions of floating point operations per second (GFlops/s), measured by counting flops over a time step and dividing by the duration of that same time step. This is a reasonable (and reproducible) measurement, because unlike for many other numerical methods, the number of flops required for simplicial DG is relatively uniquely determined. Note that because the measurement corresponds to an average, individual components of the method (such as element-local differentiation/lift) achieve significantly higher flop rates. Since the elementwise dense linear operators asymptotically (as $N \rightarrow \infty$) determine the run time, it may be reasonable to relate the measured performance to that achieved by dense matrix-matrix multiplies on this architecture. The best results achieved on an SGEMM workload on large, square matrices hover around 350 GFlops/s. It is therefore remarkable that our method achieves 250 GFlops/s on much less benignly shaped matrices, also taking into account that the method does much more varied work than simple matrix-matrix multiplies.

We would also like to comment on the progression of performance results as we vary N in Figure 27.10, and in particular the rapid rise in performance from $N = 1$

to $N = 3$. We mentioned earlier that optimal results for $N = 3, \dots, 5$ were an explicit goal of this work. Many of the finer tuning points of past sections (such as microblocking and work item coarsening) become rather unnecessary at $N \geq 6$ (because matrix sizes have grown significantly, and therefore enough work is available within each element). Compared to a simpler code (such as the one described in [13]), it is precisely these optimizations that lead to large gains at $N = 3, \dots, 5$.

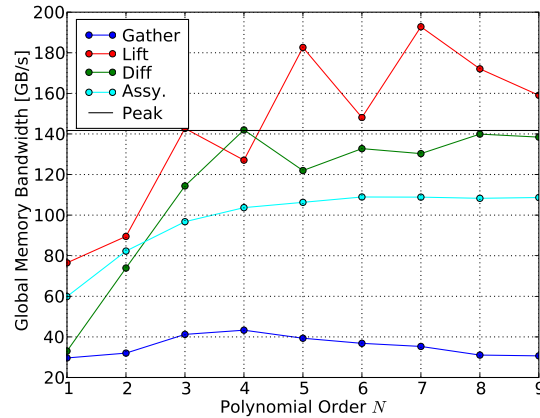


Fig. 27.11 Memory bandwidths in GB/s achieved by each part of the DG operator on an Nvidia GTX 280. The peak memory bandwidth published by the manufacturer is 141.7 GB/s. Values exceeding peak bandwidth are believed to be due to the presence of a texture cache.

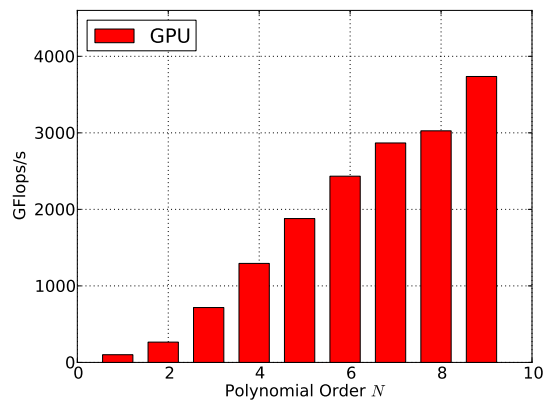
It is interesting to correlate the achieved floating point bandwidth from Figure 27.10 with the bandwidth reached for transfers between the processing cores and global memory, shown in Figure 27.11. We have obtained these numbers by counting the number of bytes fetched from global memory either directly or through a texture unit in each component of the method. The published theoretical peak memory bandwidth of the card on which this experiment was performed is 141.7 GB/s, shown as a black horizontal line. Perhaps the most striking feature here is that the calculated memory bandwidth sometimes transcends this theoretical peak. We attribute this phenomenon to the presence of various levels of texture cache. Its occurrence is especially pronounced in the case of flux lifting, and it should perhaps be sobering that the other parts of the DG operator do not manage the same feat. In any case, flux lifting uses the fields-on-chip strategy, and therefore fetches and re-fetches the rather small matrix L , making large amounts of data reuse a plausible proposition. Aside from this surprising behavior of flux lifting, it is both interesting and encouraging to see how close to peak the memory bandwidth for element-local differentiation gets. As a converse to the above, this makes it likely that the operation does not get much use out of the texture cache in most situations. It does imply, however, that rather impressive work was done by Nvidia's hardware designers: The theoretical peak global memory bandwidth can very nearly be attained in real-world computations. Next, the fact that the flux-gather part of the operator achieves rather low memory throughput is not too surprising—the access pattern is (and, for a general grid, has to be) rather scattered, decreasing the achievable bandwidth. Lastly, operator assembly, which computes linear combination of vectors, consists mainly

of global memory fetches and stores. It seems likely that ancillary operations such as index calculations, loop overhead and bounds checks drive this component’s short-fall from peak memory bandwidth.

It is worth noting that one would not initially expect a matrix-matrix workload like DG to be memory-bound, at least at high polynomial degrees N . After all, such workloads do offer large amounts of arithmetic intensity to keep floating point units busy. On the other hand, it is worth keeping in mind that there is simply *so much* floating point power available on GPU-like chips that it is quite unlikely that a code like DG might get to the point of actually being limited by it. As such, it is reasonable, in our view, to expect that for the foreseeable future, the limiting factor for most DG-like algorithms will in fact remain memory bandwidth, as evidenced by Figure 27.11.

Another issue that frequently draws questions is that of the support of double precision within GPU-like devices. Marketing pressure in this area has led GPU manufactures to increase the ratios of the number of double precision (DP) units to the number of single precision (SP) units. Current high-end offerings hover between a factor of 1/2 and 1/4, where this feature is often used to differentiate between ‘consumer-grade’ and ‘professional-grade’ hardware. We would like to remark that in bandwidth-bound applications, there is no reason to expect a DP code to go any faster than half as fast as an equivalent SP code, for the simple reason that DP numbers are exactly twice as big as SP numbers, and therefore require twice as much memory bandwidth. In addition, DP requires twice as much on-chip memory to obtain equivalent levels of data reuse—an amount that simply might not be available. With respect to DG, we observe that at low N (e.g. $N = 1, 2$), the ratio (DP GFlops/s)/(SP GFlops/s) is about a factor 1/2, as the algorithm is completely bandwidth bound. As N increases, it approaches the above-mentioned ratio of (available DP units)/(available SP units), which further substantiates the conjecture made above that the code is “underway” to being compute-bound.

Fig. 27.12 Floating point performance in GFlops/s achieved by our auto-tuning solver on a very large 3D Maxwell problem on 16 Nvidia T10 GPUs (parts of an Nvidia S1070 compute server) in single precision. Performance is calculated by measuring wall time from one time step to the next and dividing the number of flops performed (including timestepping) by this value.



Lastly, we would like to comment on Figure 27.12, which illustrates the performance of our solver in GFlops/s at various polynomial orders N on a cluster of 16

Nvidia Tesla T10 GPUs. Two features of this plot are immediately noteworthy. First, computational performance approaches 25% of the overall machine peak at $N = 9$ with nearly four teraflops/s. It is remarkable that such performance is achievable on a cluster that costs a small fraction of the large machines whose hallmark such performance was previously. Second, it is also obvious where the distributed-memory inter-node communication (via MPI in this case) is taking its toll, as one may, in principle, directly compare the shape of Figure 27.10 with that of Figure 27.12. It is obvious that there is a much steeper performance dropoff in the parallel run as N decreases than there is in the sequential performance data. This is owed to the fact that high orders are significantly heavier on element-local volume work (which scales as N^3), than on communication-heavy work dominated by degrees of freedom on faces (which scales as N^2). Thus, as there is more communication work compared to local compute work, the method incurs larger communication overhead. This is (in our opinion) quite expected, and it should be noted that even at $N = 5$, our code nearly achieves a still very respectable 2 teraflops/s on this cluster. This also contains an important message about the parallelization of DG, which holds true at both the distributed-memory and the shared-memory scale: High polynomial orders N , along with all their other benefits, also much improve the parallelizability of the method.

27.6 Conclusions

In this article, we have shown that high-order DG methods can reach double-digit percentages of published theoretical peak performance values for the hardware under consideration. This speed increase translates directly into an increase of the size of the problem that can be treated using these methods. A single compute device can now do work that previously required a roomful of computing hardware. Alternatively, a cluster of machines equipped with these cards can run simulations that were previously outside the reach of all but the largest supercomputers. This lets the size and complexity of simulations that researchers can afford on a given hardware budget jump significantly.

We find that GPU-DG is far more economical to run at medium to large scales than CPU-DG. In our opinion, this is due to the fact that the computational structure of the method, with its two levels of “element” and “individual degree of freedom”, is very well-suited to the GPU a priori—better even than finite-difference methods, which are often cited as a “GPU poster child”. Through the use of the auto-tuning technology described in this article along with a number of further tricks discussed in detail in [12], we have shown that rather good performance and machine utilization can be achieved by GPUs in DG-like workloads.

In addition to highlighting our work on GPU-DG, this article also serves to introduce the reader to the idea that scripting languages and GPUs make a good team. Beyond the core benefit of enabling run-time code generation, they also facilitate a

clear separation of the code into ‘administrative’ and ‘computational’ parts. Such a separation contributes to code clarity and helps make code more maintainable.

As we continue to explore the benefits of GPUs for DG and DG-like workloads, we will be focusing on areas such as adaptivity in both space and time, nonlinear equations, and the use of curvilinear geometries, as well as much larger scaling of GPU-DG. Initial work on these matters can be found in the articles [4, 14, 27].

We believe that GPU-DG will have a bright future, with many more applications benefiting from the ease with which large-scale time-domain simulations can be performed using DG, and we hope that our work has helped and will help application scientists use DG computations in their role as part of the ‘third pillar of science’.

Acknowledgments

AK’s research was partially funded by AFOSR under contract number FA9550-07-1-0422, through the AFOSR/NSSEFF Program Award FA9550-10-1-0180 and also under contract DEFG0288ER25053 by the Department of Energy. TW acknowledges the support of AFOSR under grant number FA9550-05-1-0473 and of the National Science Foundation under grant number DMS 0810187. JSH was partially supported by AFOSR, NSF, and DOE. The opinions expressed are the views of the authors. They do not necessarily reflect the official position of the funding agencies.

References

- [1] T. Barth and T. Knight. A Streaming Language Implementation of the Discontinuous Galerkin Method. Technical Report 20050184165, NASA Ames Research Center, 2005.
- [2] J. Bilmes, K. Asanovic, C. Chin, and J. Demmel. Optimizing matrix multiply using PHiPAC: a portable, high-performance, ANSI C coding methodology. In *Proceedings of the 11th international conference on Supercomputing*, pages 340–347. ACM, 1997.
- [3] I. Buck, T. Foley, D. Horn, J. Sugerman, K. Fatahalian, M. Houston, and P. Hanrahan. Brook for GPUs: stream computing on graphics hardware. In *Int. Conf. on Computer Graphics and Interactive Techniques*, pages 777–786. ACM New York, NY, USA, 2004.
- [4] C. Burstedde, O. Ghattas, M. Gurnis, T. Isaac, G. Stadler, T. Warburton, and L. Wilcox. Extreme-scale amr. In *High Performance Computing, Networking, Storage and Analysis (SC), 2010 International Conference for*, pages 1–12, nov. 2010. doi: 10.1109/SC.2010.25.
- [5] B. Cockburn, S. Hou, and C.-W. Shu. The Runge-Kutta Local Projection Discontinuous Galerkin Finite Element Method for Conservation Laws. IV:

- The Multidimensional Case. *Mathematics of Computation*, 54(190):545–581, 1990. doi: 10.2307/2008501.
- [6] W. J. Dally, P. Hanrahan, M. Erez, T. J. Knight, F. Labonté, J. H. Ahn, N. Jayasena, U. J. Kapasi, A. Das, and J. Gummaraju. Merrimac: Supercomputing with streams. In *Proceedings of the ACM/IEEE SC2003 Conference (SC'03)*, volume 1, 2003.
- [7] J. Filipovič and J. Fousek. Medium-grained functions mapping using modern GPUs. In *Proceedings of the Symposium on Application Accelerators in High Performance Computing (SAAHPC'11)*, Knoxville, TN, 2010.
- [8] M. Frigo and S. G. Johnson. The design and implementation of FFTW3. *Proc. IEEE*, 93(2):216–231, 2005. doi: 10.1109/JPROC.2004.840301. Special issue on “Program Generation, Optimization, and Platform Adaptation”.
- [9] D. Göddeke, R. Strzodka, and S. Turek. Accelerating double precision FEM simulations with GPUs. In *Proceedings of ASIM*, 2005.
- [10] J. S. Hesthaven and T. Warburton. *Nodal Discontinuous Galerkin Methods: Algorithms, Analysis, and Applications*. Springer, first edition, November 2007. ISBN 0387720650.
- [11] A. Klöckner, N. Pinto, Y. Lee, B. Catanzaro, P. Ivanov, and A. Fasih. PyCUDA and PyOpenCL: A Scripting-Based Approach to GPU Run-Time Code Generation. Technical Report 2009-40, Scientific Computing Group, Brown University, Providence, RI, USA, Nov. 2009. URL <http://arxiv.org/abs/0911.3456>. submitted.
- [12] A. Klöckner, T. Warburton, J. Bridge, and J. Hesthaven. Nodal discontinuous Galerkin methods on graphics processors. *J. Comp. Phys.*, 228:7863–7882, 2009. doi: 10.1016/j.jcp.2009.06.041.
- [13] A. Klöckner, T. Warburton, and J. Hesthaven. Solving Wave Equations on Unstructured Geometries. In W.-m. Hwu, editor, *GPU Computing Gems, Jade Edition*. Morgan Kaufmann Publishers, Waltham, MA, 2011.
- [14] A. Klöckner, T. Warburton, and J. S. Hesthaven. Viscous Shock Capturing in a Time-Explicit Discontinuous Galerkin Method. *Math. Model. Nat. Phenom.*, 6:57–83, 2011. doi: 10.1051/mmnp/20116303.
- [15] S. Krakowsky, L. Turner, and M. Okoniewski. Acceleration of finite-difference time-domain (FDTD) using graphics processor units (GPU). In *Microwave Symposium Digest, 2004 IEEE MTT-S International*, volume 2, pages 1033–1036 Vol.2, 2004. ISBN 0149-645X. doi: 10.1109/MWSYM.2004.1339160.
- [16] C. Lattner and V. Adve. LLVM: A Compilation Framework for Life-long Program Analysis & Transformation. *Code Generation and Optimization, IEEE/ACM International Symposium on*, 0:75, 2004. doi: 10.1109/CGO.2004.1281665.
- [17] P. Lesaint and P. Raviart. On a finite element method for solving the neutron transport equation. *Mathematical aspects of finite elements in partial differential equations*, pages 89–123, 1974.
- [18] W. Li, X. Wei, and A. Kaufman. Implementing Lattice Boltzmann computation on graphics hardware. *The Visual Computer*, 19:444–456, 2003.

- [19] E. Lindholm, J. Nickolls, S. Oberman, and J. Montrym. Nvidia Tesla: A Unified Graphics and Computing Architecture. *IEEE Micro*, 28:39–55, 2008. doi: 10.1109/MM.2008.31.
- [20] A. H. Mohammadian, V. Shankar, and W. F. Hall. Computation of electromagnetic scattering and radiation using a time-domain finite-volume discretization procedure. *Computer Physics Communications*, 68(1-3):175 – 196, 1991. doi: 10.1016/0010-4655(91)90199-U.
- [21] C. Mueller, B. Martin, and A. Lumsdaine. CorePy: High-Productivity Cell/BE Programming. In *Proc. of the First STI/Georgia Tech Workshop on Software and Applications for the Cell/BE Processor*, 2007.
- [22] Nvidia Corporation. *NVIDIA CUDA 2.2 Compute Unified Device Architecture Programming Guide*. Nvidia Corporation, Santa Clara, USA, April 2009.
- [23] T. Oliphant. *Guide to NumPy*. Trelgol Publishing, Spanish Fork, UT, July 2006.
- [24] W. H. Reed and T. R. Hill. Triangular mesh methods for the neutron transport equation. Technical report, Los Alamos Scientific Laboratory, Los Alamos, 1973.
- [25] G. van Rossum et al. The Python programming language, 1994. URL <http://python.org>.
- [26] T. Warburton. An explicit construction of interpolation nodes on the simplex. *J. Eng. Math.*, 56:247–262, 2006. doi: 10.1007/s10665-006-9086-6.
- [27] T. Warburton. A low storage curvilinear discontinuous galerkin time-domain method for electromagnetics. In *Electromagnetic Theory (EMTS), 2010 URSI International Symposium on*, pages 996–999. IEEE, 2010.
- [28] R. C. Whaley, A. Petitet, and J. J. Dongarra. Automated empirical optimizations of software and the ATLAS project. *Par. Comp.*, 27:3–35, 2001. doi: 10.1016/S0167-8191(00)00087-9.